ChemPubSoc Europe

DOI: 10.1002/open.201600135

Open Access ChemistryOPEN Communications

Step-by-Step Design and Synthesis of Au@SiO_2@Phenyl-azathiacrown for SERS-Based Specific Quantification of Inorganic Mercury

Yuchao Wu,[a] Limin Yang,[a] and Qiuquan Wang*[a, b]

Direct SERS-based quantification of inorganic metal species has been a problem, because they have a small Raman cross-section or even no vibrational mode. Here, we report a new strategy for SERS-based quantification of such metal species, as exemplified by inorganic mercury (Hg^{II}) in waters. Step-by-step design and synthesis from azathioethers [3, 9-dithia-6-monoazaundecane (DMA) and 3,6,12,15-tetrathia-9-monoazaheptadecane (TTM)] to an azathiacrown [7-aza-1,4,10,13-tetrathiacyclohexadecane (NS4)] demonstrate an improved S-pulling effect and size-fit specificity towards Hg^{II} to form Hg–S bonds. Modification of NS4 on the surface of Au@SiO_2 by using a 4-(bromomethyl)benzoic linker enabled direct SERS-based specific quantification of Hg^{II} for the first time, in which the ultrathin layer (ca. 2 nm) that covered the Au core (55 nm) could be a barrier preventing the Au core from having direct interaction with the Hg^{II}, and with phenyl serving as an internal standard (IS). The ratio of the Hg–S SERS band intensity at 270 cm^{-1} to that of IS [(γCC + γCCC) at 1046 cm^{-1}] was practically proportional to the concentration of Hg^{II}, eliminating the inevitable uncertainties encountered in SERS-based measurements. Such a methodology is expected to pave a new way for SERS-based quantification of inorganic metal species when specific complexing substrates and suitable ISs are designed.

As an affordable molecular structure information tool, surface-enhanced Raman scattering (SERS) on the roughened nanostructured surface of noble metals amplifies the orders of magnitude of Raman signals.[1] One, thus, expects such a sensitive SERS to be applicable to the quantification of not only target molecules, but also small inorganic metal species.[2] However, SERS-based quantification is still a difficult task, especially in the direct and reliable quantification of inorganic metal species. They have small Raman cross-sections or even no vibrational modes, providing almost negligible Raman signals, for example, inorganic mercury (Hg^{II}) in waters. To the best of our knowledge, almost all SERS-based methods reported for the detection of Hg^{II} are mediated by Raman reporting molecules. Interactions between Hg^{II} and the SERS reporting molecules or the SERS reporting-molecule-modified pre-adsorbed ligands lead to variation in their distance to the SERS-active substrate, causing the SERS signals to turn on or turn off.[2a,3] In this way, Hg^{II} was detected indirectly through changes in the SERS intensity or frequency of the reporting molecules, with possible uncertainties. More reliable quantification of the SERS signal that came directly from Hg^{II} itself remains challenging, when comparing with techniques that use atomic fluorescence spectrometry and inductively coupled plasma mass spectrometry.[4]

Herein, we report a new strategy for direct SERS-based quantification of the inorganic metal species, as exemplified by the specific quantification of Hg^{II}, a never out-of-date star, because its irreplaceable usefulness, but terrible toxicity, has always attracted attention. Azathioether and azathiacrown, which contain S atoms to form the quasi-covalent Hg–S bonds, were designed and synthesized step-by-step to obtain the direct Raman signal solely from the Hg–S bond. This was modified on the surface of Au@SiO_2 nanoparticles within an effective distance[5] of the enhanced electromagnetic field through a 4-(bromomethyl)benzoic linker, achieving highly sensitive SERS of Hg–S. At the same time, the phenyl moiety in the linker served as an internal standard (IS) to normalize the determined Hg–S SERS signal, which might be influenced by possible instrumental variations, less uniform distribution of the electromagnetic hot spots on the surface of SERS-active Au@SiO_2 nanoparticles, and diverse adaptations of the localized near-field microenvironment towards the samples of different physicochemical properties,[6] so as to realize a reliable SERS-based specific quantification of Hg^{II} (Scheme 1).

First, we used a simple sulfhydryl-bearing compound, 2-mercaptoethanol ($HSCH_2CH_2OH$, 2-ME), to confirm the SERS signal of Hg–S in an Au@SiO_2 nanoparticle sol-based manner (Figures S1 and S2a in the Supporting Information). The Raman band of Hg–S at 260 cm^{-1} was observed and was significantly enhanced by four orders of magnitude when $Hg(SCH_2CH_2OH)_2$ was physically mixed with the Au@SiO_2 nanoparticles (Figure S3a). Then, we started to synthesize 3,9-dithia-6-monoazaundecane (DMA, **1**) (Scheme 1 and Figure S4) and conjugated with 4-(bromomethyl) benzoic acid (**4**) to obtain 8-[*N*,*N*-

[a] Y. Wu, L. Yang, Prof. Dr. Q. Wang
Department of Chemistry
and Key Laboratory of Spectrochemical Analysis & Instrumentation
College of Chemistry and Chemical Engineering
Xiamen University, Xiamen 361005 (P. R. China)
E-mail: qqwang@xmu.edu.cn

[b] Prof. Dr. Q. Wang
State Key Laboratory of Marine Environmental Science
Xiamen University, Xiamen 361005 (P. R. China)

Supporting Information and the ORCID identification number(s) for the author(s) of this article can be found under http://dx.doi.org/10.1002/open.201600135.

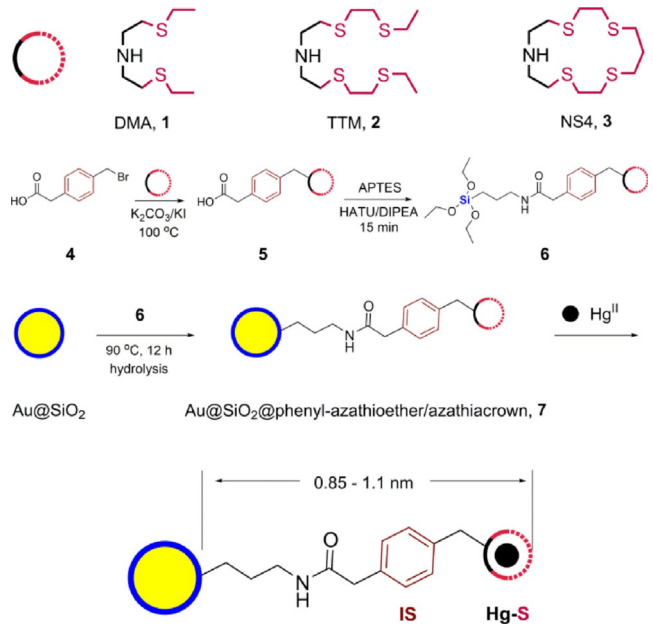

Scheme 1. Au@SiO_2@phenyl-azathioether/azathiacrown designed for the SERS-based quantification of Hg^{II}.

bis(2-(ethylthio)ethyl)aminomethyl] phenylacetic acid (phenyl-DMA, **5**) (Scheme 1 and Figure S5). Phenyl-DMA was then linked with 3-aminopropyltriethoxysilane (APTES, **6**) and anchored onto Au@SiO_2 nanoparticles (Scheme 1 and Figure S6) to obtain Au@SiO_2@phenyl-DMA (**7**) (Scheme 1). The zeta potential (ξ) of Au@SiO_2, determined by using DLS experiments, changed from -23.0 ± 0.2 to 44.8 ± 0.9 mV after phenyl-DMA modification (Table S1). Moreover, their TEM and STEM images indicated that Au@SiO_2 had a 55 nm Au core covered by an SiO_2 shell (ca. 2 nm) (Figure 1 a_1–a_5). It should be pointed out that the ultrathin SiO_2 shell can be a barrier to prevent the Au core from direct interaction with Hg^{II}. The size of Au@SiO_2@phenyl-DMA (Figures 1 b_1–b_2) did not increase obviously, owing to the length of phenyl-DMA (0.85 nm, as calculated by using the Molecular Mechnics MM2 method in ChemBio3D Ultra 14.0 software). STEM images (Figures 1 b_3–b_6) of Au@SiO_2@phenyl-DMA, especially the superimposed STEM image of Si and S (Figure 1 b_7), clearly showed the modification of S-containing phenyl-DMA on the surface of Au@SiO_2. Au@SiO_2@phenyl-DMA was subsequently used for the SERS-based quantification of Hg^{II}. The Hg–S SERS band was observed as a shoulder at 275 cm^{-1}, together with the Hg–N band at 236 cm^{-1} (Figure 2 a) that was verified by using the experiment of Hg^{II} with 2-aminoethanol ($H_2NCH_2CH_2OH$, 2-AE) (Figure S2 b). A 15 cm^{-1} shift of the Hg–S SERS band compared to that (260 cm^{-1}) in the case of 2-ME was attributed to the interaction between Hg and N in DMA that competed and, thus, perturbed Hg–S bonding. Moreover, other inorganic metal species such as Cd^{II}, Zn^{II}, Cu^{II}, Pb^{II}, Mn^{II}, Ni^{II}, Fe^{III}, and Ag^{I}, which are similar in physicochemical properties considering their interactions with S and N atoms, and possibly coexist with Hg^{II} in water samples, might be trapped together by DMA. We investigated their SERS behavior, and the observed SERS bands of Cd–N (263 cm^{-1}), Cu–N (258 cm^{-1}), and Fe–N (222 cm^{-1}) as well as Ag–N (240 cm^{-1}) and Ag–S (238 cm^{-1}) overlapped with those of Hg–N and Hg–S (Figure 2 a), indicating that Ag^{I}, Cd^{II}, Cu^{II}, and Fe^{III} interfere with the determination of Hg^{II} when using Au@SiO_2@phenyl-DMA (Figure S2 c and S2 d).

Higher bond dissociation energies of Ag–S (217 kJ mol^{-1}), Cd–S (208), Cu–S (274), Fe–S (323), and Hg–S (217) compared to those of A–N (170 kJ mol^{-1}), Cd–N (160), Cu–N (192), Fe–N (184), and Hg–N (177) (Table S2) implied that stronger interactions of these inorganic metal species with S than with N. Therefore, we considered introducing more S atoms into the DMA complexing moiety to synthesize 3,6,12,15-tetrathia-9-monoazaheptadecane (TTM, **2**) (Scheme 1) so as to pull them away from the N in TTM. This was an effective way to weaken the coordinative bond formed between the metal species and N, as evidenced by the results obtained using the synthesized Au@SiO_2@phenyl-TTM (Table S1 and Figure 1 c; its synthesis and characterization are described in Figures S7–S9). The SERS bands at 263 cm^{-1} (Cd–N), 260 cm^{-1} (Cu–N), and 222 cm^{-1} (Fe–N) as well as Hg–N and Ag–N disappeared compared to those observed in the case of Au@SiO_2@phenyl-DMA; however, Ag–S (232 cm^{-1}) and Hg–S (270 cm^{-1}) were still there with merely 6 and 5 cm^{-1} shifts, respectively (Figure 2 b). These observed phenomena indicated that the interactions between the metal species and N became negligible, confirming our consideration that more S atoms in TTM pull the metal species away from N. Elimination of the interferences from Cd^{II}, Cu^{II}, and Fe^{III} towards Hg^{II} was achieved. However, the broad bands of Ag–S and Hg–S partly overlapped, inferring that Ag^{I} still interfered with the determination of Hg^{II}. In this situation, we had to use Cl^- to get rid of Ag^{I} from the sample before SERS measurements (Figure S10), as Ag^{I} could easily be removed by forming an AgCl precipitate ($K_{sp}=1.8\times10^{-10}$); whereas, Hg^{II} formed more soluble Hg–Cl complexes, for example, the stability constants of $HgCl^+$ is 5.5×10^6 and $HgCl_2$ 1.6×10^{13},[7] along with the increase in Cl^- concentration, avoiding its co-precipitation with AgCl.

Crown molecules can recognize metal ions of different diameters by their cavity size.[8] Combining this size-fit property and the S-pulling effect on the soft metal species, as demonstrated in the case of TTM, we designed and synthesized 7-aza-1,4,10,13-tetrathiacyclohexadecane (NS4, **3**) (Scheme 1), an azathiacrown that contains four S atoms, to further improve the binding-selectivity towards Hg^{II}. It was modified onto the surface of Au@SiO_2 following the same procedures as in the cases of Au@SiO_2@phenyl-DMA and Au@SiO_2@phenyl-TTM to obtain Au@SiO_2@phenyl-NS4 (Table S1 and Figure 1 d; its synthesis and characterization are described in Figures S11–S13). The TEM and STEM images (Figures 1 d_1–d_6) as well as the superimposed STEM image of Si and S (Figure 1 d_7) confirmed the modification of phenyl-NS4 (1.1 nm as calculated with MM2) on the surface of Au@SiO_2. In addition, the ξ value of Au@SiO_2@phenyl-NS4 increased to 11.7 ± 1.5 from -23.0 ± 0.2 mV for Au@SiO_2 (Table S1). Specific recognition of Hg^{II} was realized at the SERS band of 270 cm^{-1} with four orders of magnitude signal enhancement (see Figure S3 b), whereas the SERS band of Ag–S at 232 cm^{-1} and those of other metal species were

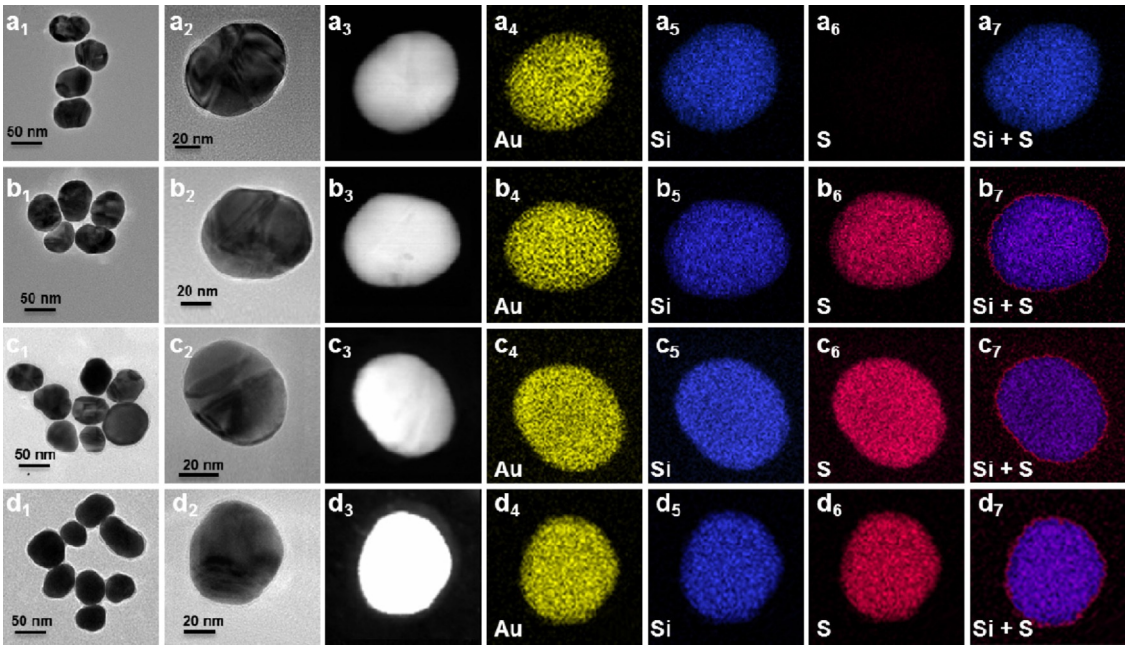

Figure 1. TEM and STEM images. a_1, a_2) TEM and a_3) STEM images of Au@SiO_2, a_4–a_6) corresponding elemental mapping (Au–M, Si–K, S–K signal), and a_7) the superimposed STEM of Si–K and S–K. b_1, b_2) TEM and b_3) STEM images of Au@SiO_2@phenyl-DMA, b_4–b_6) corresponding elemental mapping (Au–M, Si–K, S–K signal), and b_7) the superimposed STEM of Si–K and S–K. c_1, c_2) TEM and c_3) STEM images of Au@SiO_2@phenyl-TTM, c_4–c_6) corresponding elemental mapping (Au–M, Si–K, S–K signal), and c_7) the superimposed STEM of Si–K and S–K. d_1, d_2) TEM and d_3) STEM images of Au@SiO_2@phenyl-NS4, d_4–d_6) corresponding elemental mapping (Au–M, Si–K, S–K signal), and d_7) the superimposed STEM of Si–K and S–Kl.

not detected, as shown in Figure 2c. The formed Hg^{II} chelate was verified by using mass spectroscopy (Figure 3). Hg^{II} was coordinated in the chemical form of $Hg(OH)_2$ [phenyl-NS4-$Hg(OH)_2$, *m/z* 710] with the precise isotope distribution pattern based on the theoretical estimation using IsoPro 3.0 software. This was in agreement with the fact that the predominant species of Hg^{II} in natural water is $Hg(OH)_2$ (stability constant is 1.0×10^{22}) with an approximate linear configuration.[9] Moreover, theoretical minimized-energy calculations with MM2 indicated that the distance between the diagonal sulfur atoms in the phenyl-NS4 cavity was 5.878 and 7.666 Å for ^{4}S to ^{11}S and ^{7}S to ^{14}S, respectively (Figure S14a). After coordinating to $Hg(OH)_2$, the distance between ^{4}S and ^{11}S decreased to 4.832 Å for ^{4}S–Hg–^{11}S with a bond angle of 148.3°, and that of ^{7}S to ^{14}S decreased to 4.900 Å for ^{7}S–Hg–^{14}S with a bond angle of 154.9° (Figure S14b). These configuration changes were for size-fit recognition, considering that the radius of Hg^{2+} is 1.02 Å and each Hg–S bond length was 2.510 Å in the octahedral configuration, in which $Hg(OH)_2$ with the HO–Hg–OH bond angle of 154.1° was almost vertically coordinated into the cavity (Figure S14b). It is worth pointing out that the approximate linear configuration and vertical-style insert of $Hg(OH)_2$ into the azathiacrown was crucial for Hg^{II}-specific coordination and recognition, regardless of the fact that Hg^{II} might associate with other anions in some real water samples when concentrations of the anions were abnormally high, such as Cl^- in seawater. For Ag^{I}, however, a more energetic cost (47.81 kcal mol^{-1}) compared to that in the case of Hg^{II} (22.50 kcal mol^{-1}) was needed to form ^{4}S–Ag–^{11}S with a bond angle of 126.0°, and ^{7}S–Ag–^{14}S with 119.7°. The rigid azathiacrown NS4 had to be distorted seriously in order to reach the smaller distances of ^{4}S–Ag–^{11}S (4.199 Å) and ^{7}S–Ag–^{14}S (4.076 Å), owing to the shorter Ag–S bond length 2.354–2.359 Å (Figure S14c), resulting in an unstable state.

The water certificated reference material (CRM) GSBZ 50016-90:202037 was used to validate the feasibility of our proposed strategy for a direct SERS-based specific quantification of Hg^{II} in waters using Au@SiO_2@phenyl-NS4. For accurate quantification, a good IS should be placed in the same situation together with the targeted analyte. This is particularly important for SERS-based quantitative analysis, because the intensity of the SERS signals suffers from the uncertainties arising from possible instrumental variations, distribution uniformity of the electromagnetic hot spots on the surface of the SERS-active substrate, and their unequable adaptation microenvironment towards the samples of different physicochemical properties, as discussed above. The phenyl moieties that link NS4 and Au@SiO_2 (Scheme 1) were fully exposed to the same near-field microenvironment as the extracted Hg^{II}, and thus the area ratio (A_{Hg-S}/A_{phenyl}) of the Hg–S SERS band at 270 cm^{-1} to the typical phenyl band (γCC + γCCC) at 1046 cm^{-1} could normalize the uncertainties (Figure 4a). The obtained results demonstrated the necessity of phenyl as an IS when the calibration curve was plotted with A_{Hg-S}/A_{phenyl} compared to A_{Hg-S} alone (Figure 4b). The dynamic concentration linear range of Hg^{II} against A_{Hg-S}/A_{phenyl} was from 0.4 to 2.0 ng mL^{-1} (higher concentrations were not tested) with a correlation coefficient of 0.991 and an RSD of 7.4% at 1.0 ng mL^{-1} ($n=5$), whereas that of Hg^{II} concentration against A_{Hg-S} alone began to bend at 1.0 ng mL^{-1} with insupportable fluctuations. In this way, the

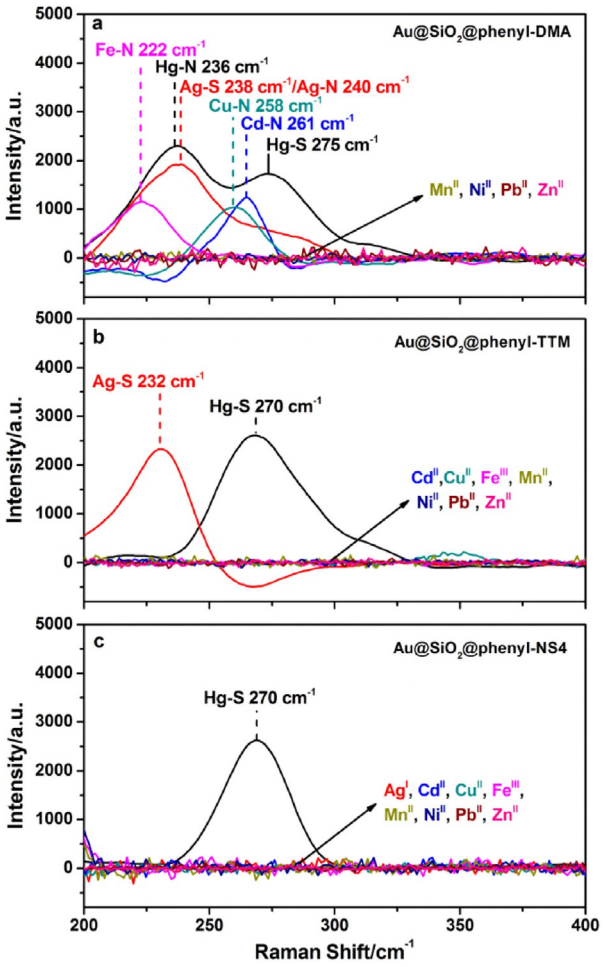

Figure 2. SERS spectra. a) Au@SiO_2@phenyl-DMA-(Hg^{II}, Ag^{I}, Cd^{II}, Cu^{II}, Fe^{III}, Mn^{II}, Ni^{II}, Pb^{II}, and Zn^{II}); b) Au@SiO_2@phenyl-TTM-(Hg^{II}, Ag^{I}, Cd^{II}, Cu^{II}, Fe^{III}, Mn^{II}, Ni^{II}, Pb^{II}, and Zn^{II}); c) Au@SiO_2@phenyl-NS4-(Hg^{II}, Ag^{I}, Cd^{II}, Cu^{II}, Fe^{III}, Mn^{II}, Ni^{II}, Pb^{II}, and Zn^{II}). The Au@SiO_2@phenyl-DMA, Au@SiO_2@phenyl-TTM, and Au@SiO_2@phenyl-NS4 used were 3 mg mL^{-1} and the metal species Hg^{II}, Ag^{I}, Cd^{II}, Cu^{II}, Fe^{III}, Mn^{II}, Ni^{II}, Pb^{II}, and Zn^{II} used were 1 μg mL^{-1} each. Laser: 785 nm; power: 3 mW; exposure time: 10 s. All the data presented were those after subtracting the background determined when using Au@SiO_2 NPs alone. Each point is the mean of five duplicate experiments.

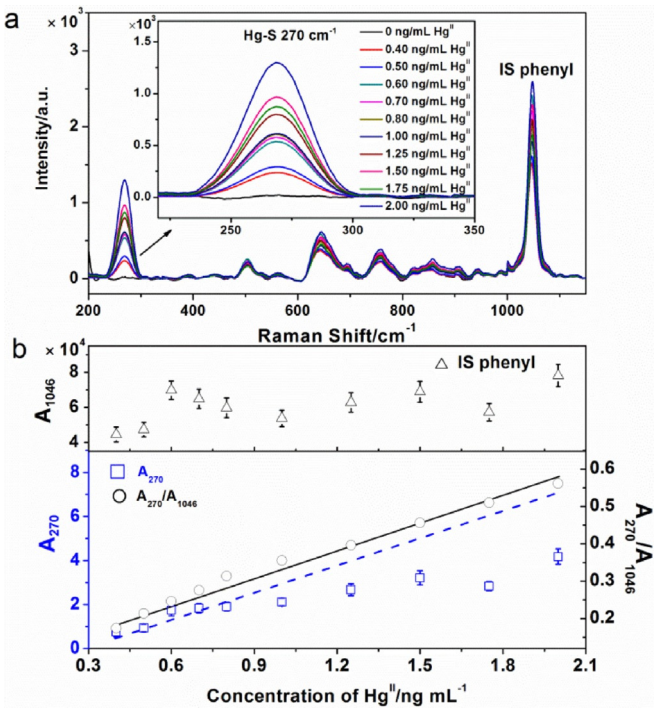

Figure 4. a) SERS spectra obtained in the presence of different concentrations of Hg^{II} using Au@SiO_2@phenyl-NS4. b) Fluctuation of the SERS intensity of IS phenyl, and the calibration curves of Hg^{II} concentration against the intensity ratio of Hg–S SERS band at 270 cm^{-1} to phenyl band at 1046 cm^{-1} (black line), as well as the intensity of Hg–S SERS band at 270 cm^{-1} alone (blue dash line). The Hg^{II} concentrations tested were 0.40, 0.50, 0.60, 0.70, 0.80, 1.00, 1.25, 1.50, 1.75, and 2.00 ng mL^{-1}, whereas 3 mg mL^{-1} Au@SiO_2@phenyl-NS4 was used. Laser: 785 nm; power: 3 mW; exposure time: 10 s. All the data presented were those after subtracting the background determined when using Au@SiO_2 NPs alone. Each point is the mean of five duplicate experiments.

limit of detection (3σ) reached 0.09 ng mL^{-1} and the limit of quantification (10 σ) was 0.31 ng mL^{-1}, satisfactorily meeting the basic requirement for safe drinking water [the threshold values of Hg^{II} are 6 ng mL^{-1} (WHO),[10] 2 ng mL^{-1} (USEPA),[11] and

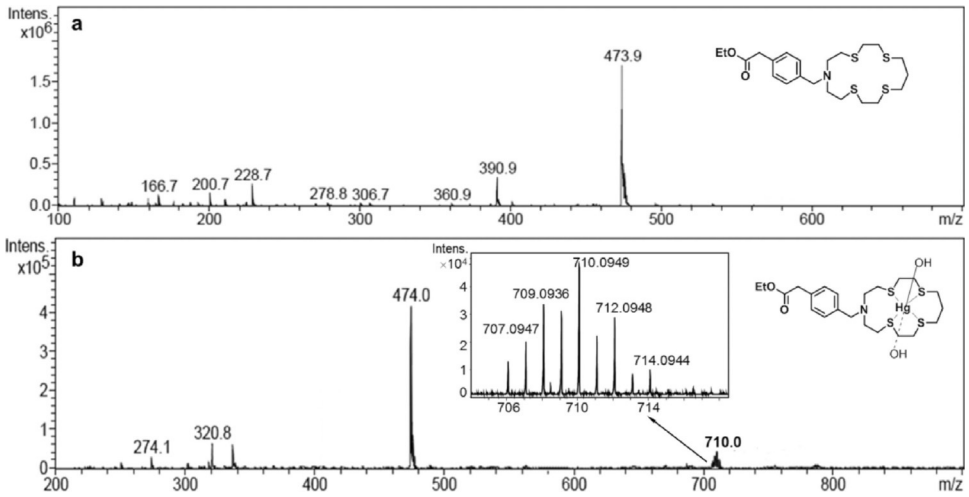

Figure 3. ESI–MS spectra of ethyl-esterified phenyl-NS4 before (a) and after (b) coordination with Hg^{II}. The inset shows the enlarged isotopic distribution of ethyl-esterified phenyl-NS4-$Hg(OH)_2$ around *m/z* 710.

1 ng mL^{-1} (SAC)[12]]. The determined concentration of Hg^{II} in the CRM was 11.5 ± 1.0 ng mL^{-1} (n = 5). It was well in accordance with the certificated value (11.9 ± 1.2 ng mL^{-1}), confirming an accurate SERS-based quantification of Hg^{II} using the designed Au@SiO_2@phenyl-NS4. It was applied to measure Hg^{II} in fresh water samples collected from the Ting River, which flows from Fujian through Guangdong province, and in the seawater around Xiamen Island, southeastern China (Figure S15).

In summary, we have demonstrated the step-by-step design and synthesis of Au@SiO_2@phenyl-azathioether/azathiacrown for direct SERS-based specific quantification of Hg^{II} for the first time, in which the intensity ratio of the Hg–S SERS band (270 cm^{-1}) to the IS phenyl band (1046 cm^{-1}) directly reflected the Hg^{II} concentration, achieving a reliable SERS-based quantification of Hg^{II} in various waters. Not limited to Hg^{II}, we believe that the methodology reported in this manuscript sets an example for the SERS-based quantification of other inorganic metal species, whereby specific complexing substrates and suitable ISs are designed and synthesized. Moreover, not restricted to Au@SiO_2 nanoparticles, the channel surfaces in a microfluidic chip that are chemically modified with SERS-active nanostructures are expected to perform a more efficient SERS-based quantification of Hg^{II} and other inorganic metal species in the near future.

Acknowledgements

We thank the National Instrumentation Program of China (2011YQ03012401), the National Basic Research 973 Project (2014CB932004), and the National Natural Science Foundation of China (21535007, 21475108 and 21275120) as well as the Foundation for Innovative Research Groups of the National Natural Science Foundation of China (21521004) and Program for Changjiang Scholars and Innovative Research Team in University (PCSIRT, IRT13036) for financial support. We thank Dr. Jianfeng Li, Dr. Deyin Wu, Dr. Huaizhi Kang, Dr. Bin Ren and Dr. Zhongqun Tian (XMU) and Dr. Yongguang Yin, Dr. Yong Cai, and Dr. Guibin Jiang (CAS) for helpful discussion, instrumentation, and experimental assistance. Professor John Hodgkiss is thanked for his assistance with English language polishing.

Conflict of Interest

The authors declare no conflict of interest.

Keywords: azathiacrown · azathioether · gold nanoparticle · mercury · surface-enhanced Raman scattering

[1] P. L. Stiles, J. A. Dieringer, N. C. Shah, R. P. Van Duyne, *Annu. Rev. Anal. Chem.* **2008**, *1*, 601 – 626.
[2] a) R. A. Alvarez-Puebla, L. M. Liz Marzan, *Angew. Chem. Int. Ed.* **2012**, *51*, 11214 – 11223; *Angew. Chem.* **2012**, *124*, 11376 – 11385; b) W. Shen, X. Lin, C. Jiang, C. Li, H. Lin, J. Huang, S. Wang, G. Liu, X. Yan, Q. Zhong, B. Ren, *Angew. Chem. Int. Ed.* **2015**, *54*, 7308 – 7312; *Angew. Chem.* **2015**, *127*, 7416 – 7420.
[3] a) J. Huber, K. Leopold, *TrAC Trends Anal. Chem.* **2016**, *80*, 280 – 292; b) C. Song, B. Yang, Y. Yang, L. Wang, *Sci. China Chem.* **2016**, *59*, 16 – 29.
[4] a) Method 1631, Revision E: Mercury in Water by Oxidation, Purge and Trap, and Cold Vapor Atomic Fluorescence Spectrometry, Environmental Protection Agency, U.S., Washington DC, **2002**; b) Y. M. Yin, J. Liang, L. M. Yang, Q. Q. Wang, *J. Anal. At. Spectrom.* **2007**, *22*, 330 – 334; c) Y. G. Yin, J. F. Liu, B. He, J. B. Shi, G. B. Jiang, *J. Chromatogr. A* **2008**, *1181*, 77 – 82; d) D. Yan, L. M. Yang, Q. Q. Wang, *Anal. Chem.* **2008**, *80*, 6104 – 6109; e) A. D'Ulivo, J. Dedina, Z. Mester, R. E. Sturgeon, Q. Q. Wang, B. Welz, *Pure Appl. Chem.* **2011**, *83*, 1283 – 1340; f) H. M. Li, Z. G. Xu, L. M. Yang, Q. Q. Wang, *J. Anal. At. Spectrom.* **2015**, *30*, 916 – 921.
[5] a) G. J. Kovacs, R. O. Loutfy, P. S. Vincett, C. Jennings, R. Aroca, *Langmuir* **1986**, *2*, 689 – 694; b) J. R. Anema, J. F. Li, Z. L. Yang, B. Ren, Z. Q. Tian, *Annu. Rev. Anal. Chem.* **2011**, *4*, 129 – 150.
[6] S. E. Bell, N. M. Sirimuthu, *Chem. Soc. Rev.* **2008**, *37*, 1012 – 1024.
[7] G. S. James, *Lange's Handbooks of Chemistry, 16th ed.*, McGRAW-HILL, INC., New York, **2005**.
[8] a) J. J. Christensen, J. O. Hill, R. M. Izatt, *Science* **1971**, *174*, 459 – 467; b) J. S. Bradshaw, R. M. Izatt, *Acc. Chem. Res.* **1997**, *30*, 338 – 345.
[9] a) X. Wang, L. Andrews, *Inorg. Chem.* **2005**, *44*, 108 – 113; b) K. J. Powell, P. L. Brown, R. H. Byrne, T. Gajda, G. Hefter, S. Sjoeberg, H. Wanner, *Pure Appl. Chem.* **2005**, *77*, 739 – 800.
[10] *Guidelines for drinking-water quality, 4th ed.*, WHO, Geneva, Switzerland, **2011**.
[11] 2012 Edition of the Drinking Water Standards and Health Advisories, Environmental Protection Agency, U.S., Washington DC, **2012**.
[12] Standards for Drinking Water Quality, Ministry of Public health and Standardization Administration and of the People's Republic of China, Beijing, **2006**.

Received: October 27, 2016
Revised: November 28, 2016
Published online on March 1, 2017

